

Simulation and Derivation of Deflection Equation for Suspended Diaphragm for MEMS Application Using Kirchhoff-Love Theory

Mohammad Reza Mahlooji¹

Javad Koohsorkhi²

¹M.S student, Faculty of New Sciences& Technologies, University of Tehran, Tehran, Iran

mrmahlooji@ut.ac.ir

²Assistant Professor, Advanced Micro and Nano Devices Lab., Faculty of New Sciences& Technologies, University of Tehran, Tehran, Iran

koohsorkhi@ut.ac.ir

Abstract:

In this paper, using theory of sheets, the deflection of suspended diaphragm has been obtained under uniform and circular loading. This type of diaphragm, unlike other diaphragms, has a central support which is recommended to be used in MEMS applications. The relationship between diaphragm deflection and static analysis of this diaphragm enjoys a great significance in investigating and understanding its behavior and calculating its other practical parameters both in dynamic and static fields. Here, using the thin sheet Kirchhoff-Love theory these issues are addressed. The results of analysis and simulation have been compared with each other, representing the 1% accuracy of the obtained statements, suggesting accuracy of the obtained results. The results show that the suspended diaphragm has greater deflection compared to simple flat diaphragm, which is considered important in sensors and micro electromechanical devices.

Keywords: Deflection equation, Kirchhoff-Love Theory, Suspended diaphragm, Uniform loading, Annular loading, Finite Element Simulation

Submission date : 20, 07, 2017

Acceptance date : 23, 05, 2018

Corresponding author : J. Koohsorkhi

Corresponding author's address: North Karegar Ave. Fnst, Mems Dep., University of Tehran, Tehran, Iran.



1. Introduction

Sheets are one of the suitable options in many applications. Analysis of the behavior of sheets on their loading helps designers to evaluate and optimize their structure. In the first time in 1776, Euler examined sheets theoretically and analyzed their free vibration [1]. Bernoulli, based on Euler theory, assuming that sheets are a set of beams, tried to analyze sheets, but he did not find satisfactory results. French Germean stated an independent differential equation for the sheet. Then, Lagrange in 1813 corrected it and considered the term which was not included in Germean equations. However, for the first time Kuchi and Poisson in 1829 formulated sheet bending equations based on theory of elasticity, which were in line with Lagrange results. Nevertheless, Navier by considering the thickness of sheet and its effect on bending stiffness D presented the correct relationship, and converted differential relations to algebraic expressions through Fourier relations. In 1850, Kirchhoff published a thesis and stated two basic and independent assumptions, through which he analyzed thin sheets. Lord Kelvin and Tit converted torsion couple to shear force on the edges and considered shear force and bending moment at any edge, thereby correcting Kirchhoff assumptions [2-3]. Recently, with the development of science and technology, these findings of the recent century have attracted a great deal of attention for new devices. One of the newly emerging in the current century is MEMS technology, in which diaphragms are widely used in different forms for barometers, microphones, and actuators [4-5]. So far, three types of diaphragms known as simple, grooved, and embossed have been introduced, which are used for different purposes. In all these type of diaphragms, the support encompasses the diaphragm environment. In this paper, a design is presented and investigated in which the support is located in the center of the diaphragm, which is known as suspended diaphragm. This diaphragm has various uses in detecting sound waves. After colliding with this diaphragm, a sound wave causes the deflection on the edges, where this deflection can be measured by common reading mechanisms [6]. In reference [7], aembossed diaphragm whose circumference has been attached to the body has been examined, which is used in pressure sensors working in closed and vacuum systems. Suspended diaphragm can be applied in MEMS instruments, sensors, and actuators as upward and downward according to Fig. 1. Mechanically, both have the same analysis. This diaphragm is especially useful for sensors that are important in terms of mechanical force effect including pressure, sound, or flow. In this paper, static investigation of this type of diaphragm is investigated under different loadings, and the results are compared with finite element method through COMSOL software.

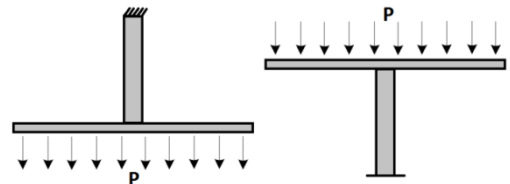


Fig. 1. Two different modes of loading for suspended diaphragm.

2. Principles of basic theory of deflection of diaphragms

The behavior of sheets is such that they mostly tolerate the transverse load with bending. For this reason, bending stiffness and the torsional stiffness of sheet art important characteristics of sheets to bear the load exerted to them. Sheet stiffness depends on its thickness. Therefore, in order to investigate the theory of sheets, they are categorized into three groups in terms of dimensions/thickness ratio. The sheets are either thick, or thin, or too thin which are called membrane [8].

Kirchhoff-Law plane theory is a two-dimensional mathematical model used for determining the stress and deformity of thin planes undergoing force or momentum. Kirchhoff assumptions include basic assumptions dealing with investigating small deflection of the sheet. This theory is also known as classic theory of thin planes. Here, we use Kirchhoff-Law assumptions, and solve the problem assuming that the diaphragm thickness is small in relation to other dimensions. The first assumption of Kirchhoff-Law is that the deflection of the middle surface W remains without strain in comparison to the small plane thickness and in response to bending. The second assumption states that the stress perpendicular to the middle surface is negligible in comparison to the other elements of the stress and indeed the planes perpendicular to the middle surface remain perpendicular to the middle surface after bending. In addition, the loading should be such that it develops deflection by at most 10% of the diaphragm thickness in it. This extent of deflection is equal to a deviation of less than 1% from the linearity assumption of deflection and pressure relationship [8]. If the extent of deflection of the sheet is small against the thickness of the small sheet, the sheet deflection follows Eq. (1) [9]:

$$\nabla^4 w = P \quad (1)$$

If the load exerted to the circular diaphragm and its boundary conditions are symmetrical and independent of θ , the deflection of diaphragm W will be only dependent on r , where these conditions are called symmetric bending of the sheet. In this case, $M_{r\theta}$ and Q_θ are zero and only M_r , M_θ , and Q_r should be considered. Therefore, the general Eq. (1) is simplified to Eq. (2) [9]:

$$\frac{d}{dr} \left[\frac{1}{r} \frac{d}{dr} \left(r \frac{dw}{dr} \right) \right] = -\frac{Q_r}{D} \quad (2)$$

Q_r is the shear force per surface area unit and D represents the bending stiffness of the sheet, which are equal to the following respectively [9]:

$$Q_r = \frac{1}{2\pi r} \int_0^{2\pi} \int_0^r Pr dr d\theta = \frac{Pr}{2} \quad (3)$$

P is the intensity of the exerted load and r shows the distance from the circle center [9]:

$$D = \frac{Et^3}{12(1-\nu^2)} \quad (4)$$

In the above relation, E is the Young modulus, t shows the sheet thickness, and ν represents Poisson coefficient. Differential equation (2) has a specific solution resulting from Q_r plus a general solution. The specific solution of the equation is determined based on the sheet loading, and is obtained by substituting Relation (3) into (2). The general solution of the equation which is solved assuming zero input of Eq. (2) is in the form of Relation (5) [9]:

$$w_h = \frac{C1}{4}r^2 + C2\ln r + C3 \quad (5)$$

Relation (5) holds true for each part of the diaphragm with any kind of boundary conditions, loading, and geometric conditions. Thus, along the radius of a diaphragm, if geometric or loading conditions changed, a separate deflection equation should be considered for each region, and continuity boundary conditions should also be considered for every boundary between them. Eventually, the diaphragm deflection is the sum of their specific and general solutions:

$$W = W_h + W_p \\ = \frac{C1}{4}r^2 + C2\ln r + C3 + W_p \quad (6)$$

The constants in Relation (5) are obtained by applying boundary conditions to Relation (6). Boundary conditions are of two types: 1) static boundary conditions involving deflection and deflection slope at support boundaries as well as continuity between the two regions and center; 2) dynamic boundary conditions covering the shear force and moment. The central boundary conditions:

$$W'(r=0) = 0 \quad (7)$$

This condition always makes $C2$ coefficient in Relation (5) zero.

2.1. Continuity Boundary Conditions

In the boundary of all regions in which they geometric and loading conditions of the diaphragm are changed, the deflection, deflection slope, and moment are equal with each other.

The effective moment, shear force, and transverse force for circular sheet under axial symmetrical loading are obtained from Relations (8)-(10), respectively [9,10]:

$$M_r = -D \left[\frac{d^2w}{dr^2} + \frac{\nu}{r} \frac{dw}{dr} \right] \quad (8)$$

$$Q_r = -D \frac{d}{dr} \left[\frac{d^2w}{dr^2} + \frac{1}{r} \frac{dw}{dr} \right] \quad (9)$$

$$V_r = Q_r + \frac{1}{r} \frac{\partial M_{r\theta}}{\partial \theta} \quad (10)$$

2.2. Boundary Conditions of Support

Based on the constraints governing the sheet movement at external boundaries which are fixed or free (no support) or as see-saw movement, its boundary conditions are according to Table 1.

Table 1. Different types of support boundary conditions

Type of support	Condition 1	Condition 2
Simple	$w = 0$	$M_r = 0$
Fixed	$w = 0$	$w' = 0$
Free (No support)	$M_r = 0$	$V_r = 0$

Here, the support boundary conditions are of free type, which has been stiffened in the center. The general solution of the equation is the sum of general and specific solution, and it is the specific solution to the input form which should satisfy differential equation (2) with Q_r input.

At free edges, M_r , Q_r , and $M_{r\theta}$, are zero where r is the direction perpendicular to the plane and t is the direction tangential to the plane. On the other hand, in classic theory or Kirchhoff-Law, two conditions are met, to resolve which an approximate relation was presented by Kirchhoff. Since the moment at the free edge is zero, i.e. $M_n=0$, but due to the curvature of free edge, $M_{r\theta}$ should also be zero, thus by approximating the torsional moment of the edge with transverse shear force, Kirchhoff presented the second condition of the free edge as Relation (11) known as equivalent shear force [9,10]:

$$V_r = Q_r + \frac{1}{r} \frac{\partial M_{r\theta}}{\partial \theta} \quad (11)$$

3. Suspended Diaphragm under Transverse Loading

Considering the usage of diaphragm in pressure sensors, suspended diaphragm deflection is investigated under two types of loading: 1) uniform loading on the entire surface of the diaphragm; 2) loading on a circular region.

3.1. Suspended Diaphragm under Uniform Loading

Assuming that the diaphragm radius is c and the radius of its central support is b , attached to a fixed support at the boundary of b , while being free and suspended at the boundary of c , the diaphragm loading under uniform load will be as Eq. (12):

$$Q_{r,s.u} = \frac{Pr}{2} \quad (12)$$

The specific solution resulting from this loading which is obtained by satisfying the main equation is as follows [9]:

$$W_{p,s.u} = \frac{P}{64D} r^4 \quad (13)$$

Fig. 2 represents the uniform loading plus parameters and boundary conditions. As can be observed, the arrows lie uniformly on the entire surface of the diaphragm, representing uniform load.

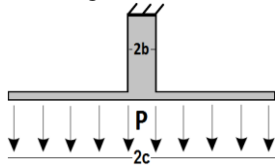


Fig. 2. Loading mechanism and boundary condition in uniform loading.

When applying the boundary conditions, the general solution and coefficients are obtained from Relations (14), which is the suspended diaphragm deflection equation with uniform loading:

$$W = \frac{C1_{s.u}r^2}{4} + C2_{s.u} \log(r) + C3_{s.u} - \frac{Pr^2(8c^2 - 8c^2 \log(r) + r^2)}{64D_1} \quad (14)$$

Where, the coefficients of this equation can be calculated by the following relations:

$$C1_{s.u} = \frac{A0 + A2a^2 + A4a^4}{B0 + B2a^2} \quad (15)$$

Where, the coefficients of Eq. (15) can be calculated as Eqs. (16).

$$\begin{aligned} A0 &= b^4(1 - \nu) \\ A2 &= 2b^2(1 - \nu) - 4b^2 \log(b)(1 - \nu) \\ A4 &= (1 + 3\nu) - 4 \log(a)(1 + \nu) \\ B0 &= -8D_1 b^2(\nu - 1) \\ B2 &= 8D_1(\nu + 1) \end{aligned} \quad (16)$$

Also:

$$C2_{s.u} = \frac{A2a^2 + A4a^4}{B0 + B2a^2} \quad (17)$$

Where, the coefficients of Eq. (17) can be calculated as Eqs. (18):

$$\begin{aligned} A2 &= b^4(\nu + 1) \\ A4 &= 4b^2 \left(\log\left(\frac{a}{b}\right) \right) (\nu + 1) - b^2(\nu - 1) \end{aligned}$$

$$\begin{aligned} B0 &= -16D_1 b^2(\nu - 1) \\ B2 &= 16D_1(\nu + 1) \end{aligned} \quad (18)$$

and:

$$C3_{s.u} = \frac{A0 + A2a^2 + A4a^4}{B0 + B2a^2} \quad (19)$$

Where, the coefficients of Eq. (19) can be calculated by Eqs. (20):

$$\begin{aligned} A0 &= b^6(\nu - 1) \\ A2 &= b^4(5 - 3\nu) - 4b^4 \log(b)(\nu + 1) \\ A4 &= 8b^2 \log(a)(\nu + 1) + 4b^4 \log(b)(\nu + 3) \\ &\quad + b^2(\nu + 3) \\ &\quad + 16b^2 \log(b^2)(\nu + 1) \\ &\quad - 16b^2 \log(a)\log(b)(\nu + 1) \\ B0 &= -64D_1 b^2(\nu - 1) \\ B2 &= 64D_1(\nu + 1) \end{aligned} \quad (20)$$

According to Eq. (14), the diagrams of Figs. 3-6 the accuracy of the obtained theoretical relationship and the results of simulation have been compared. As seen in Fig. 3, the more we move farther away from the support, the extent of diaphragm deflection grows, and the bending behavior of the diaphragm changes linearly at farther points from the support.

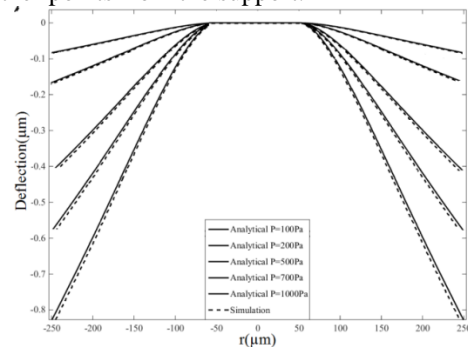


Fig. 3. Deflection of circular diaphragm under different and uniform pressures, $c=250\mu\text{m}$, $b=50\mu\text{m}$ and $t=2.5\mu\text{m}$.

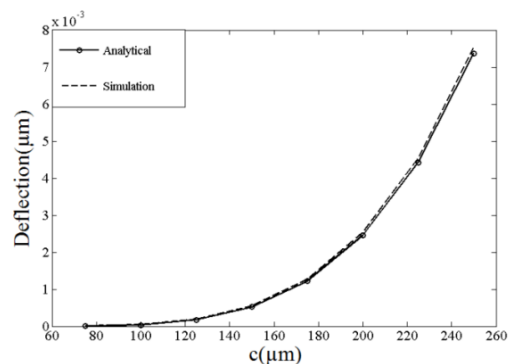


Fig. 4. Deflection of circular diaphragm under uniform loading with different diaphragm radius, $P=10\text{Pa}$, $b=50\mu\text{m}$ and $t=2.5\mu\text{m}$.

Fig. 5 demonstrates the effect of the support radius. As can be observed, the more the radius of the support part increases, the extent of deflection diminishes

dramatically since the rigid part of the diaphragm grows.

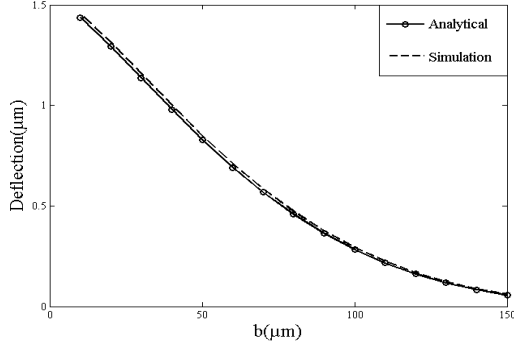


Fig. 5. Deflection of circular diaphragm under uniform loading with different support radius, $P=1000\text{Pa}$, $a=250\mu\text{m}$ and $t=2.5\mu\text{m}$.

Fig. 6 demonstrates the effect of the diaphragm thickness. As can be seen, this thickness plays a significant role in the extent of deflection of the diaphragm. As the diagram thickness becomes larger than $4\mu\text{m}$, the extent of deflection becomes trivial. Therefore, to use this structure in sensor usages, thicknesses smaller than $4\mu\text{m}$ should be used.

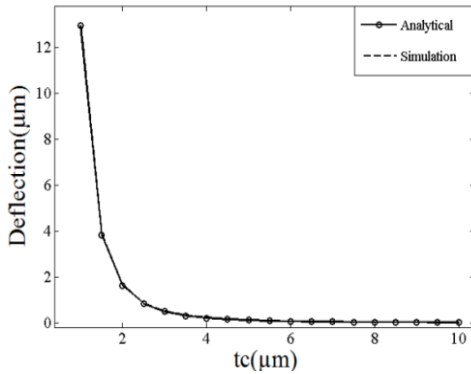


Fig. 6. Deflection of circular diaphragm under uniform loading with different diaphragm thickness, $P=1000\text{Pa}$, $b=50\mu\text{m}$ and $a=250\mu\text{m}$.

3.2. Suspended Diaphragm under Circular Loading

In this case, a load as circular with internal radius of d and external radius of f has been considered, such that $c > f > d > b$. In this condition, three types of structural and loading regions should be considered. The entire structure is viewed in three regions: the internal region $b < r < d$, middle region $d < r < f$ and external region $f < r < c$, represented by Indices 1, 2, 3, respectively. Region 3 does not have any special changes at this loading. Fig. 7 demonstrates the manner of loading, parameters, and boundary conditions. The place of arrows in this figure which is circular represents the manner of applying circular load.

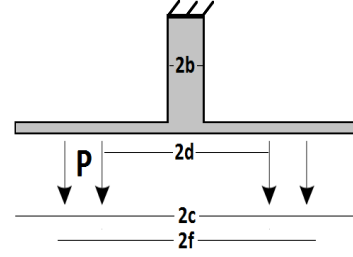


Fig. 7. Circular loading mechanism and parameters.

In this condition, where the loading is circular, the loading for each region is:

$$\begin{aligned} Q_{r,s,r}^{(1)} &= \frac{P(f^2 - d^2)}{2r} \\ Q_{r,s,r}^{(2)} &= \frac{P(r^2 - d^2)}{2r} \\ Q_{r,s,r}^{(3)} &= 0 \end{aligned} \quad (21)$$

The specific solution of the mentioned loadings is as follows, respectively:

$$\begin{aligned} W_{p,s,r}^{(1)} &= \frac{Pr^2(\ln r - 1)(d^2 - f^2)}{8D} \\ W_{p,s,r}^{(2)} &= \frac{Pr^2(8f^2 - 8f^2 \ln r + r^2)}{64D} \\ W_{p,s,r}^{(3)} &= 0 \end{aligned} \quad (22)$$

The boundary conditions are fixed at edge b and free at edge c . In boundaries d and f , continuity conditions should hold true among the equations. Accordingly, the continuity conditions are as follows:

$$\begin{aligned} W_{s,r}^{(3)}(r=f) &= W_{s,r}^{(2)}(r=f) \\ W'_{(3)s,r}(r=f) &= W'_{(2)s,r}(r=f) \\ M_{r,s,r}^{(3)}(r=f) &= M_{r,s,r}^{(2)}(r=f) \\ W_{s,r}^{(2)}(r=d) &= W_{s,r}^{(1)}(r=d) \\ W'_{(2)p,s,r}(r=d) &= W'_{(1)p,s,r}(r=d) \\ M_{r,s,r}^{(2)}(r=d) &= M_{r,s,r}^{(1)}(r=d) \end{aligned} \quad (23)$$

Given the boundary conditions and continuity conditions, the general equation of the suspended diaphragm deflection with circular loadings and the internal region $b < r < d$ is obtained as follows:

$$W_1 = \frac{C11_{ce.u.e}r^2}{4} + C21_{ce.u.e} \log(r) + C31_{ce.u.e} - \frac{Pr^2(\log(r) - 1)(d^2 - f^2)}{8D_1} \quad (24)$$

Where, that shear moment is as follows:

$$M_r = -D \left[\frac{d^2 w}{dr^2} + \frac{v}{r} \frac{dw}{dr} \right] \quad (25)$$

By applying boundary conditions, the coefficients of the general equation become as follows:

$$C11_{ce.u.e} = \frac{A0 + A2a^2}{B0 + B2a^2} \quad (26)$$

Where, the coefficients of Eq. (26) can be calculated by Eqs. (27):

$$\begin{aligned} A0 &= f^4(v-1) - d^4(v-1) + 2b^2d^2(v-1) \\ &\quad - 2b^2f^2(v-1) \\ &\quad + 4b^2d^2 \log(b)(v+1) \\ &\quad - 4b^2f^2 \log(b)(v+1) \\ A2 &= 2f^2(v+1) - 2d^2(v+1) \\ &\quad + 4d^2 \log(d)(v+1) \\ &\quad - 4f^2 \log(f)(v+1) \\ B0 &= -8D_1b^2(v-1) \\ B2 &= 8D_1(v+1) \end{aligned} \quad (27)$$

Also:

$$C21_{ce.u.e} = \frac{A0 + A2a^2}{B0 + B2a^2} \quad (28)$$

Where, the coefficients of Eq. (28) can be obtained as Eqs. (29):

$$\begin{aligned} A0 &= (b^2f^4 - b^2d^4)(1-v) \\ A2 &= 4b^2d^2 \log\left(\frac{b}{d}\right)(v+1) \\ &\quad - 4b^2f^2 \log\left(\frac{b}{f}\right)(v+1) \\ B0 &= -16D_1b^2(v-1) \\ B2 &= 16D_1(v+1) \end{aligned} \quad (29)$$

And:

$$C31_{ce.u.e} = \frac{A0 + A2a^2}{B0 + B2a^2} \quad (30)$$

Where, the coefficients of Eq. (30) can be calculated by Eqs. (31):

$$\begin{aligned} A0 &= b^2d^4(v-1) + 2b^4d^2(v-1) \\ &\quad - b^2f^4(v-1) - 2b^4f^2(v-1) \\ &\quad + 2b^2d^4 \log(b)(v+1) \\ &\quad - 2b^2f^4 \log(b)(v+1) \\ A2 &= 2b^2f^2(v+1) - 2b^2d^2(v+1) \\ &\quad + 4b^2d^2 \log\left(\frac{b}{d}\right)(v+1) \\ &\quad - 8b^2f^2(v+1)(\log(b) \log(f) \\ &\quad - \log(b)^2) \\ &\quad - 8b^2d^2(\log(b)^2 \\ &\quad - \log(b) \log(d))(v+1) \\ &\quad - 4b^2f^2 \log\left(\frac{b}{f}\right)(v+1) \\ B0 &= -32D_1b^2(v-1) \\ B2 &= 32D_1(v+1) \end{aligned} \quad (31)$$

Considering the boundary conditions of Eq. (23), the general equation of the suspended diaphragm

deflection with circular loading is obtained in the middle region $d < r < f$:

$$W_2 = \frac{C12_{ce.u.e}r^2}{4} + C22_{ce.u.e} \log(r) + C32_{ce.u.e} \frac{Pr^2(8f^2 - 8f^2 \log(r) + r^2)}{64D_1} \quad (32)$$

By applying boundary conditions, the coefficients of the general equation for this region are:

$$C12_{ce.u.e} = \frac{A0 + A2a^2}{B0 + B2a^2} \quad (33)$$

Where, the coefficients of Eq. (33) can be calculated by Eqs. (34):

$$\begin{aligned} A0 &= -d^4(v-1) + f^4(v-1) - 2b^2f^2(v-1) \\ &\quad - 4b^2d^2 \log\left(\frac{b}{d}\right)(v-1) \\ &\quad + 4b^2f^2 \log(b)(v-1) \\ A2 &= 2f^2(v+1) - 4f^2 \log(f)(v+1) \\ B0 &= -8D_1b^2(v-1) \\ B2 &= 8D_1(v+1) \end{aligned} \quad (34)$$

Also:

$$C22_{ce.u.e} = \frac{A0 + A2a^2}{B0 + B2a^2} \quad (35)$$

Where, the coefficients of Eq. (34) can be calculated as Eqs. (35):

$$\begin{aligned} A0 &= -b^2f^4(v-1) \\ A2 &= d^4(v+1) + 4b^2d^2 \log\left(\frac{b}{d}\right)(v+1) \\ &\quad - 4b^2f^2 \log\left(\frac{b}{f}\right)(v+1) \\ B0 &= -16D_1b^2(v-1) \\ B2 &= 16D_1(v+1) \end{aligned} \quad (36)$$

And:

$$C32_{ce.u.e} = \frac{A0 + A2a^2}{B0 + B2a^2} \quad (37)$$

Where, the coefficients of Eq. (37) can be calculated as Eqs. (38):

$$\begin{aligned} A0 &= 4b^4d^2(v-1) - 3b^2d^4(v-1) \\ &\quad - 2b^2f^4(v-1) - 4b^4f^2(v-1) \\ &\quad + 4b^2d^4 \log\left(\frac{b}{d}\right)(v+1) \\ &\quad - 4b^2f^4 \log(b)(v+1) \end{aligned}$$

$$\begin{aligned}
A2 = & 5d^4(v + 1) - 4b^2d^2(v + 1) \\
& + 4b^2f^2(v + 1) \\
& + 8b^2d^2 \log\left(\frac{b}{d}\right)(v + 1) \\
& - 16b^2d^2(\log(b))^2 \\
& - \log(b) \log(d)(v + 1) \\
& - 16b^2f^2(v + 1)(\log(b) \log(f) \\
& - \log(b)^2) - 4d^4 \log(d)(v + 1) \\
& - 8b^2f^2 \log\left(\frac{b}{f}\right)(v + 1)
\end{aligned}
\tag{38}$$

In the diagrams of Figs. 8-12, the accuracy of the above relations has been shown using COMSOL simulation tools. The results in Figs. 8-10 represent that the behavior of this type of loading (circular loading) is the same as uniform loading, and only the extent of the diaphragm deflection has been lower in this type of loading.

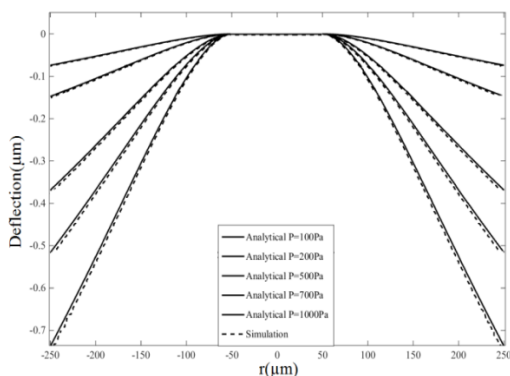


Fig. 8. Deflection of circular diaphragm under circular loading in different pressure, $c=250\mu\text{m}$, $b=50\mu\text{m}$ and $t=2.5\mu\text{m}$.

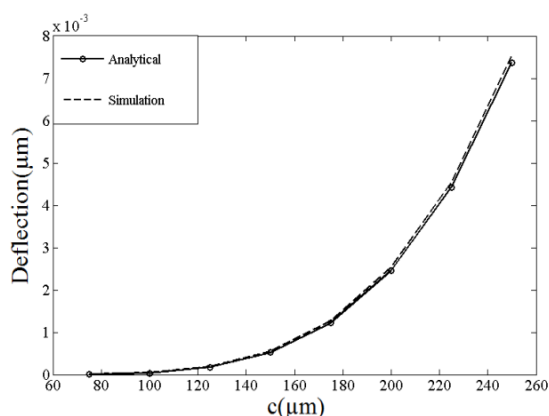


Fig. 9. Deflection of circular diaphragm under circular loading in different diaphragm radius, $P=10\text{Pa}$, $f=c$, $b=50\mu\text{m}$, $d=150\mu\text{m}$ and $t=2.5\mu\text{m}$.

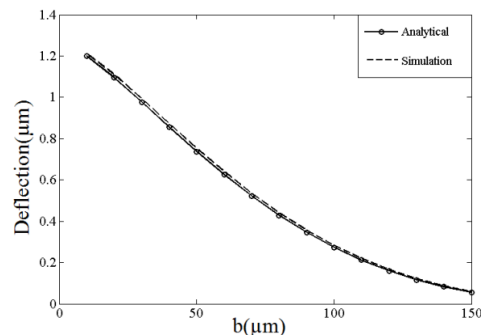


Fig. 10. Deflection of circular diaphragm under circular loading in different support radius, $P=1000\text{Pa}$, $f=c$, $c=250\mu\text{m}$, $d=150\mu\text{m}$ and $t=2.5\mu\text{m}$.

Fig. 11 demonstrates that the more the circle of load exertion moves farther away from the support, the extent of deflection grows, but from $150\mu\text{m}$ beyond, the effect of this parameter diminishes. Further, as the regional load exertion becomes narrower, the extent of deflection reaches saturation.

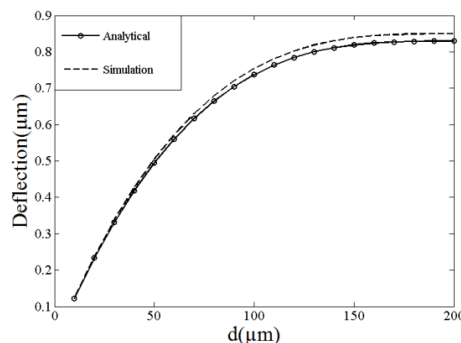


Fig. 11. Deflection of circular diaphragm under circular loading in different support radius, $P=1000\text{Pa}$, $f=c$, $c=250\mu\text{m}$, $b=50\mu\text{m}$ and $t=2.5\mu\text{m}$.

Fig. 12 indicates that as the load exertion circle becomes widened, the extent of deflection grows almost linearly. This suggests that the linear behavior emerges at farther points from the support.

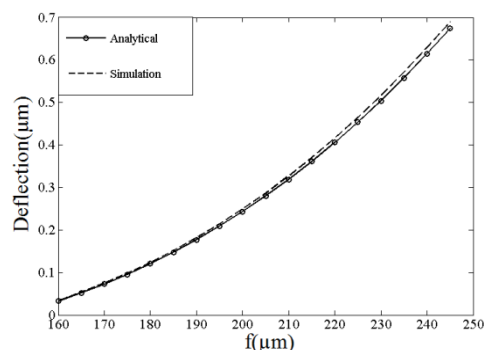


Fig. 12. Deflection of circular diaphragm under circular loading in different outer radius of loading, $P=1000\text{Pa}$, $b=50\mu\text{m}$, $c=250\mu\text{m}$, $d=150\mu\text{m}$ and $t=2.5\mu\text{m}$.

4. Comparing the Simple and Suspended Diaphragm

The main difference between the suspended diaphragm and other diaphragms is the freeness of its circumference, while its fixedness in the center. This represents the flexibility of the diaphragm. In addition, due to the increase in the flexible circumference, the sum of total deflection of the surface is far greater than that of typical diaphragms. Fig. 13 compares the maximum deflection of suspended and simple diaphragms. As can be seen, the maximum deflection of the suspended diaphragms is almost twice as large as that of the simple diaphragm. This is considered a major advantage for sensors and operators that are dependent on that movement and deflection of diaphragms.

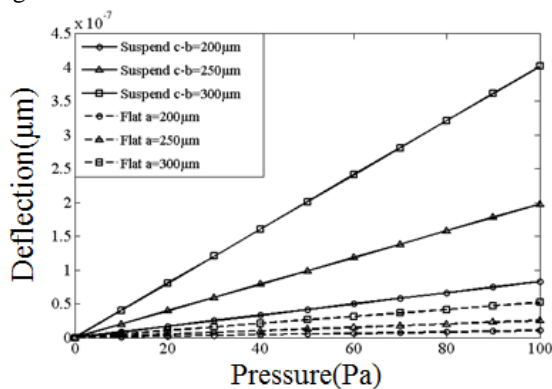


Fig. 13. Comparison of deflection between simple and suspended diaphragm.

Fig. 14 shows that some of the total displacement of the diaphragm surface. The total deflection of the diaphragm means the changes in the capacitor capacity in capacitive sensors or the total sum of pressure exerted to the pumps. As can be observed, for suspended diaphragm with support radius of $50\mu\text{m}$, it is around eight times that of the simple diaphragm with the same dimensions. This suggests that a capacitive sensor with suspended diaphragm is eight times equivalent to the simple diaphragm.

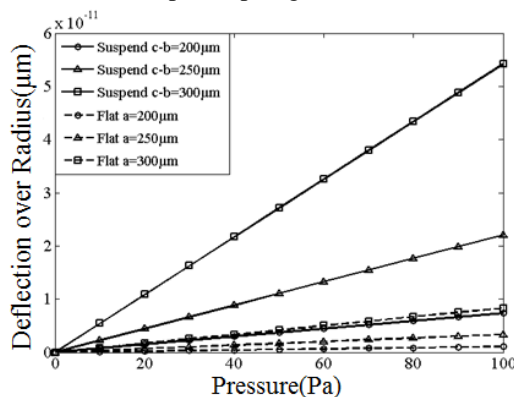


Fig. 14. Comparison of total deflection between simple and suspended diaphragm.

5. Conclusion

In this paper, suspended diaphragm, a diaphragm attached from the middle to the support was introduced for making MEMS devices and was then analyzed by classic theory. Also, the accuracy of the relations was examined using finite element methods. The high accuracy of diagrams up to the error of at most 1% proves the accuracy of the obtained theories. In the part of comparing suspended and simple diaphragms, it was observed that the maximum deflection and sum of deflection are greater in the suspended diaphragm as compared to the simple diaphragm. In different uses, sensors and operators, this represents the advantage of suspended diaphragm.

References

- [1] Euler, Leonhard. De motuvibratoriotypanorum, Novi CommentariAcadPetroplit, vol.10, pp. 243-260, 1766.
- [2] Timoshenko, Stephen, History of strength of materials: with a brief account of the history of theory of elasticity and theory of structures. Courier Corporation, 1953.
- [3] Truesdell, Clifford, Essays in the History of Mechanics, Springer Science & Business Media, 2012.
- [4] Esfandyari, M., Asadi, R., Heidari, P., Shamsi, A., "Fabrication of Electrostatic Microactuator with SU-8 polymer for continuous diaphragm-based devices", Electronics Industries, Vol. 6/3, pp. 81-87, 2015.
- [5] Nabovati, H., Mafinezhad, A., Hosseyn, k., Comprehensive Electromechanical Analysis of MEMS Variable Gap Capacitors, Journal of Iranian Association of Electrical and Electronics Engineers, vol 2.4, 2017.
- [6] Delaram, S., Haj Ghasem, H., Erfanian, A.R., Aliahmadi, M.R., "Design and Simulation of Capacitive RF MEMS Switch on Alumina Substrate", Journal of Iranian Association of Electrical and Electronics Engineers, vol 12.2, pp. 15-24, 2015.
- [7] Mahlooji, M. R., Koohsorkhi, J., "Finite Element Method for Deflection of Embossed Diaphragm" International Conference on New Achievemnets in mechanics, Industrial and Aerospace Engineering, 2016.
- [8] Sun, Yan, et al., Center embossed diaphragm design guidelines and Fabry-Perot diaphragm fiber optic sensor, Microelectronics Journal, vol. 39.5, pp. 711-718, 2008.
- [9] Timoshenko, Stephen P., and SergiusWoinowsky-Krieger. Theory of plates and shells. McGraw-hill, 1959.
- [10] M. YariEsbouei, Y. Hezarjaribi and B. A. Ganji, Simulation and Modeling of a High Sensitivity Micro-electro-mechanical Systems Capacitive Pressure Sensor with Small Size and Clamped Square Diaphragm, IJE Transaction C: Aspects Vol. 30, No. 6, pp. 846-850, 2017.